

# Large positive magnetic susceptibility of nanotube torus

Ryo Tamura

*Faculty of engineering, Shizuoka University, Johoku 3-5-1, Hamamatsu 432-8561, Japan*

Mitsuhiro Ikuta, Toru Hirahara and Masaru Tsukada

*Department of Physics, Graduate School of Science, University of Tokyo, Hongo 7-3-1,*

*Bunkyo-ku, Tokyo 113, Japan*

## Abstract

We calculate the magnetic moment caused by the persistent currents in polygonal carbon nanotube tori by the tight binding model. The polygonal CNT tori are formed by introducing heptagonal and pentagonal defects along the inner hole and outer fringe, respectively. We found a new type of large paramagnetic persistent current caused by the semi-metallic band structures of the periodic CNT junction. It is contrasted with the persistent current originated from the metallic band structure.

In spite of diamagnetism of the graphite, this paramagnetism is caused by not only the magnetic flux in the inner hole (AB flux) but also the magnetic flux directly penetrating the graphite plane (direct flux). This magnetic moment is close to that calculated with only Aharonov Bohm effect where the direct flux is included in the AB flux.

## I. INTRODUCTION

In spite of semi-metallic nature of the graphite, the carbon nanotube (CNT) becomes metallic and semi-conducting depending on the radius and the helicity of the honeycomb lattice. [1] This promising feature in nanotechnology is caused by the quantum size effect;

the system smaller than the coherent length shows electronic states different from those of the macroscopic system. Another example of the quantum size effect can be seen in the persistent current of the mesoscopic ring. An ideal clean mesoscopic one-dimensional metal ring is diamagnetic when the number of the electron is  $4n + 2$  with an integer  $n$ , while it is paramagnetic otherwise. [2] It means that the ring can have opposite sign of the magnetic susceptibility compared to the bulk system. We should notice that this positive magnetic susceptibility is inversely proportional to the temperature, i.e., it becomes divergent at the absolute zero temperature. [2–4] Though it seems similar to the Curie-Weiss rule, the origin is not the spin but the persistent current. As there is no general terminology for this paramagnetism, we call it giant orbital paramagnetism (GOP) in the present paper.

We are interested in the CNT ring discovered recently for the following reasons. [5] As for the magnetic susceptibility with respect to the magnetic field perpendicular to the honeycomb plane, the CNTs and the graphite show similar negative values, [6] whereas the persistent current of the CNT ring can show the GOP. [4] Furthermore in order to make the radius of the ring  $R$  nanometer-sized, the CNT ring will be more suitable than the conventional mesoscopic ring of metals or GaAs/AlGaAs. [7] Motivations to downsize the persistent current ring are as follows; (1) The circulating persistent current  $I$  equals  $ev_F/(2\pi R)$  with Fermi velocity  $v_F$ , and is related to the magnetic moment per ring  $M$  as  $M = I\pi R^2$ . In the rings closed-packed, therefore, the magnetic moment per unit area is proportional to  $I$  and can be increased by shrinking  $R$ . (2) The persistent current occurs on condition that the coherent length  $l_\phi$  is larger than  $2\pi R$ . Since  $l_\phi$  decreases as the temperature rises, the persistent current can be observed at higher temperature as  $R$  decreases.

In other theoretical works on the persistent current of the CNT ring, both the 'disclination' and the 'direct flux' are not considered, [4,8–10] whereas we consider both of them. Shrinking the radius of the CNT ring  $R$  increases importance of these two factors. Firstly it is explained for the disclination as follows. Figure 1 illustrates a 'polygonal CNT torus' where pentagonal and heptagonal defects form the corner of the polygonal shape along the outer fringe and the inner fringe, respectively. These defects are generally called disclinations

and have significant effect on the CNT junction, [11] the CNT cap [12] and the helical CNT. [13,14] Here we define a 'polygonal' CNT torus as the CNT torus with the disclinations, though it can also have a rounded shape when the disclinations are close to each other. [15] Only few attempts have so far been made at the persistent current of the polygonal CNT torus [16] in contrast to that of the 'circular CNT tori' discussed by many authors. [4,8–10] Here we define a 'circular' CNT torus as the CNT torus formed by elastic deformation of the straight CNT with no disclination. In the circular CNT tori, the honeycomb lattice shrinks along the tube axis with a factor  $R_1/(R_1 + D)$  at the inner fringe compared to that at the outer fringe. Here  $R_1$  and  $D$  denote the radius of the inner hole and the diameter of the CNT, respectively. Though this axial strain is relaxed to a certain degree by the elastic deformation called 'buckling', [17] it will not be enough to keep the stability if  $R_1$  is close to  $D$ . In Fig.1, on the other hand, this strain is relaxed by decreasing the number of hexagons along the inner hole side. Though it is widely known that the impurity reduces the GOP, [3,8] the effect of the disclination on the GOP is open to question. [3,4,8–10] Secondly, the importance of the direct flux is explained as follows. We consider both the magnetic flux in the graphite plane and that in the inner hole while other researchers have investigated only the latter flux. We call the former flux 'direct flux' and the latter flux 'AB flux' because the former touches the electron directly and the latter induces the Aharonov-Bohm effect. Ratio of the AB flux to the direct flux is  $R_1^2$  to  $(R_1 + D)^2 - R_1^2$ . This ratio indicates that the direct flux cannot be neglected when  $R_1$  is comparable to  $D$ . Because the graphite is diamagnetic under the direct flux, we have to find out whether the direct flux reduces the GOP. In order to clarify these open questions, we discuss the influence of the disclination and the direct flux on the magnetic moment of the polygonal CNT torus.

## II. TIGHT BINDING MODEL

When the polygonal CNT torus is composed of only semi-conducting CNTs, it has finite HOMO-LUMO gap. As can be known later, it means that the GOP does not appear.

Thus our discussion can be limited to the metallic CNTs. As first examples, we discuss the polygonal CNT torus with symmetry  $D_{6h}$  formed out of the armchair CNTs which are metallic irrespective of their radii. We use the tight binding (TB) model with only  $\pi$  orbital. The position of the atom is given by the assumed polygonal shape of the torus.

Figure 2 illustrates a part of the projection map of a polygonal CNT torus. The torus is composed of six unit cells, one of which is represented by the rectangle  $ABB'A'$ . The prime ' means that points  $X'$  and  $X$  become identical when actual three dimensional shape is formed. Vector  $\vec{L}$  denotes the circumference of the original armchair CNT. The length and direction of the CNT axis per unit cell along the outer fringe (inner fringe) is represented by  $\vec{S}$  ( $\vec{S}_2$ ). The  $i$  membered ring disclination is formed at  $P_i$  and  $Q_i$  ( $i = 5, 7$ ) by removing the shaded area and sticking the lines  $P_5P_7$ ,  $P_7D'$ ,  $DQ_7$  and  $Q_7Q_5$  on the lines  $P_5P'_7$ ,  $P'_7C'$ ,  $CQ'_7$  and  $Q'_7Q_5$ , respectively. The disclinations approximately keep the  $sp^2$  bonds of carbon atoms, i.e., the number of nearest neighbors is three for each atom. In spite of the unchanged local structure, the phase of the wave function is shifted when the electron circulate around the disclination owing to excess or deficiency of the  $\pi/3$  angle on the projection map. This topological effect cannot be represented by the effective potential energy or modification of the bond strength.

Because of the  $D_{6h}$  symmetry,  $\vec{R}_{55}$  and  $\vec{R}_{77}$  are parallel to  $\vec{L}$ , while  $\vec{S}_2$  and  $\vec{S}$  are perpendicular to  $\vec{L}$ , where the definition of  $\vec{R}_{i,j}$  is clearly illustrated in Fig.2. Thus the four integer parameters,  $n_L = |\vec{L}|/(\sqrt{3}a)$ ,  $n_{75} = |\vec{R}_{75}|/a$ ,  $n_S = |\vec{S}|/a$  and  $n_{77} = |\vec{R}_{77}|/(\sqrt{3}a)$  specify the CNT torus with  $a \simeq 0.25$  nm being lattice constant of the graphite. For example, these parameters are  $n_L = 6$ ,  $n_S = 5$ ,  $n_{75} = 2$  and  $n_{77} = 2$  in Fig.2. To keep the bond lengths almost constant, the cross section cut along  $P_5P_7Q_7Q_5P_5$  has to be rectangular, so the four integers have to satisfy the condition  $n_{77} = (n_L - n_{75})/2$ . We choose the uniform magnetic field  $\vec{B}$  parallel to the six-fold rotational axis of the torus. In Fig.2,  $B_\perp$  denotes the component of  $\vec{B}$  perpendicular to the projection map.

The unit cells are numbered along the CNT axis with  $n_1$  as shown in Fig.1. Figure 2 shows labels of atoms in each unit cell,  $(n_2, n_3)$ , where  $n_2$  specifies the zigzag rows along the

tube axis. At the inner hole side,  $n_2 = 1$  ( $n_2 = -1$ ), and  $n_2$  increases (decreases) one by one as the zigzag row climbs up (down) the inner hole wall and approaches outer fringe. In  $n_2$  zigzag row, atoms are numbered along the CNT axis as  $n_3 = 1, 2, \dots, q(n_2)$ . For example,  $q(1) = q(2) = 6, q(3) = 7$  in Fig.2. Between the neighboring unit cells, atoms  $(n_1, n_2, 1)$  and  $(n_1, n_2, q(n_2))$  connect with atoms  $(n_1 - 1, n_2, q(n_2))$  and  $(n_1 + 1, n_2, 1)$ , respectively. With this label, matrix elements of Hamiltonian between atoms  $n$  and  $m$  are represented by

$$H(B)_{n,m} = -t_{n,m} \exp(i\beta(n, m)B) . \quad (1)$$

Each atom  $n$  has a constant hopping integral  $-t_{n,m} = -t$  ( $\sim -3\text{eV}$ ) with the three nearest neighbors  $m$  and  $t_{n,m} = 0$  with all the other atoms  $m$ . The effect of the magnetic fields is included by Peierls phases  $\beta(n, m)B$ , [18] where

$$\beta(n, m) = \gamma_D(n, m)C_1 + \gamma_{AB}(n, m)C_2 \quad (2)$$

$$C_1 = \sqrt{3}\pi a^2 / (2\phi_0) ,$$

$$C_2 = \sqrt{3}\pi |\vec{S}_2|^2 / (2\phi_0) .$$

$$\gamma_{AB}(n, m) = \delta_{n_2, m_2} (\delta_{n_1, m_1+1} \delta_{n_3, 1} \delta_{m_3, q(n_2)} - \delta_{n_1, m_1-1} \delta_{m_3, 1} \delta_{n_3, q(n_2)}) ,$$

$$\begin{aligned} \gamma_D(n, m) = \delta_{n_2, m_2} \{ & f(n_2) (\delta_{q(n_2)n_1+n_3, q(n_2)m_1+m_3+1} \\ & - \delta_{q(n_2)n_1+n_3, q(n_2)m_1+m_3-1}) + g(n_2) \gamma_{AB}(n, m) \} , \end{aligned}$$

with the magnetic flux quantum  $\phi_0 = h/e$  and Kronecker delta  $\delta$ . Here  $f$  and  $g$  are linear or constant as a function of  $n_2$ ;

$$f(n_2) = \begin{cases} n_{75} & \cdots |n_2| \geq 1 + n_{75} + n_{77} \\ |n_2| - n_{77} - 0.5 & \cdots n_{77} + 1 \leq |n_2| \leq n_{75} + n_{77} \\ 0 & \cdots |n_2| \leq n_{77} \end{cases} \quad (3)$$

$$g(n_2) = \begin{cases} 0 & \cdots |n_2| \geq 1 + n_{75} + n_{77} \\ f(n_2) + 2 \sum_{j=|n_2|+1}^{n_{75}+n_{77}} f(j) & \cdots |n_2| \leq n_{75} + n_{77}. \end{cases} \quad (4)$$

In eq.(2),  $\gamma_D(i; j)C_1$  and  $\gamma_{AB}(i; j)C_2$  come from the direct flux and the AB flux, respectively. Equation (2) satisfies the condition that  $\phi_0 B \sum_{i=1}^{j-1} \beta(n^{(i+1)}; n^{(i)}) / (2\pi)$  equals the magnetic flux surrounded by the closed loop  $n^{(1)} \rightarrow n^{(2)} \rightarrow \dots \rightarrow n^{(j)} = n^{(1)}$ .

### III. RESULT

Firstly we explain the origin of the GOP of the circular CNT torus with the dispersion relation  $E_l(k, B)$  of the straight CNT under the uniform magnetic field  $B$  perpendicular to the tube axis. Ajiki and Ando showed that the direct flux flattens the dispersion lines near the Fermi level. [18] This is schematically shown by the dashed curves  $E_l(k, B)$  compared to the linear dispersion  $E_l(k, 0)$  in Fig.3. When the lattice distortion is neglected, the energy level of the circular CNT torus  $\epsilon_{l,j}$  can be expressed by

$$\epsilon_{l,j} = E_l(k_j(B), B) \quad (5)$$

$$k_j(B) = \{j + (BS_{AB}/\phi_0)\}/R \quad (6)$$

with the area of the inner hole  $S_{AB}$  and an integer  $j$ . Equation (6) represents the AB effect while difference between  $E_l(k_j(B), B)$  and  $E_l(k_j(B), 0)$  comes from the direct flux. Then the total energy  $U(B)$  is obtained as

$$U(B) = 2 \sum_{l,j} f_{\text{FD}}(\epsilon_{l,j}) \epsilon_{l,j} \quad (7)$$

where  $f_{\text{FD}}$  is Fermi-Dirac distribution function and factor 2 represents spin degeneracy. Zeeman effect is neglected here but will be discussed latter. We consider the case of the absolute zero temperature, so  $\sum_{l,j} f_{\text{FD}}$  is replaced by the summation  $\sum_{l,j=occ}$  limited to the occupied states.

The magnetic moment per torus  $M$  is calculated as  $M = -dU/dB$ . In order to see the effect of the direct flux, we firstly discuss the magnetic moment induced by only AB flux

$$M_{\text{AB}} = -S_{\text{AB}}/(R\phi_0) \sum_{l,j=occ} (dE_l(k, 0)/dk)|_{k=k_j(0)} . \quad (8)$$

Since  $E_l(k, 0)$  is an even function of  $k$ , the energy level at  $k = k_j(0)$  and that at  $k = k_{-j}(0) = -k_j(0)$  are occupied at the same time. Their contribution to  $M_{\text{AB}}$  usually cancels each other, because  $dE_l(k, 0)/dk$  is an odd function of  $k$ . When the highest occupied level (HOL) comes at K and K' corner points, however, this cancellation does not occur so that

the GOP is induced. This is illustrated in Fig.3 where the energy levels and its change caused by the AB effect are indicated by circles and arrows, respectively. Without the direct flux, the levels move along the linear dispersion line and only the level with negative  $dE/dk$  is occupied (closed circle) while that with positive  $dE/dk$  becomes vacant (open circle). Only the former contributes to the magnetic moment and brings about the giant orbital paramagnetism (GOP). The occupation of only the state with a negative  $dE/dk$  corresponds to the generation of the persistent current. The essential point is that the corner point is *partially* occupied (gray circle). If the corner point were *fully* occupied, the open circle level would be also occupied and it would cancel the energy decrease of the closed circle level. With the direct flux, however, the closed circle level is located on the dashed curve and shifted upward compared to the case without the direct flux, i.e., the direct flux reduces the GOP.

The magnetic moment for the polygonal torus can be calculated almost the same way as the circular torus. In this case, we use the phase  $\alpha$  instead of the crystal wave number  $k$ . Rotation by  $\pi/3$  with respect to the six-fold symmetry axis is equivalent to multiplying the wave function by the phase factor  $\exp(i\alpha)$  as seen in Fig.1. Though  $k\pi R/3$  corresponds to  $\alpha$ , it should be noted that  $R$  cannot be defined uniquely for the polygonal torus. The energy levels  $E_l(\alpha)$  are the eigen values of the matrix  $H_1(B) + \exp(i\alpha)H_2(B) + \exp(-i\alpha)H_2^\dagger(B)$  where  $H_1$  and  $H_2$  refer to the bonds in the unit cell and those connecting the neighboring unit cells, respectively. They are obtained from the Hamiltonian matrix  $H$  as  $H_1(n_2, n_3; m_2, m_3) \equiv H(n_1, n_2, n_3; n_1, m_2, m_3)$ , and  $H_2(n_2, n_3; m_2, m_3) \equiv H(n_1, n_2, n_3; n_1 + 1, m_2, m_3)$  with the label of atoms  $(n_1, n_2, n_3)$  defined in section II. Because the wave function is invariant under  $2\pi$  rotation,  $\alpha$  takes discrete values  $\alpha_j = (\pi/3)(j + (BS_{AB}/\phi_0))$  ( $j = \text{integer}$ ) including the AB flux,  $BS_{AB} = B3\sqrt{3}|\vec{S}_2|^2/2$ . It results in discrete levels  $E_l(\alpha_j, B)$  of the CNT torus.

On the other hand,  $E_l(\alpha, B)$  with continuous  $\alpha$  represents the continuous energy spectra of the periodic CNT junction made by connecting the unit cell of the CNT torus. In the present case, the band structure  $E_l(k, 0)$  is classified by three parameters,  $n_S/3, n_{75}/3$  and  $(n_S - n_{75})/3$  as listed in Table I according to Ref. [13]. As shown in Fig.2, the CNT torus

contains two kinds of CNTs. One is the original armchair CNT with the chiral vector  $\vec{L}$ , and the other is characterized by different chiral vector  $\vec{L}'$ . When  $n_{75}/3$  is an integer, latter becomes also metallic and we proved analytically that types 1 and 2 are semi-conducting and metallic, respectively. [14] Though we obtained only numerical results for the other types, we can say that they tend to be semi-conducting as the axial length of the semi-conducting CNT segment  $|\vec{L}' \times \vec{R}_{77}|/|\vec{L}'|$  becomes longer. [19]



TABLES

TABLE I.

$n_{75}/3$				
integer		non-integer		
$n_S/3$		$n_S/3$		
integer	non-integer	integer	non-integer	
			$(n_S - 2n_{75})/3$	
			integer	non-integer
type 1	type 2	type 3	type 4-1	type 4-2
semi-conductor	metal	semi-metal semi-conductor metal	semi-metal semi-conductor metal	semi-conductor

The dispersion curves are shown for type 2 periodic CNT junction (metallic) in Fig.4 and for type 3 periodic CNT junction (semi-metallic) in Fig.5. The index  $l$  of  $E_l(\alpha, B)$  is defined as  $E_1(\alpha, B) \leq E_2(\alpha, B) \leq \dots \leq E_{2N}(\alpha, B)$ , where  $2N$  is the number of atoms in the unit cell, i.e.,  $N \equiv 2(n_{5L}n_{7L} - n_{57}n_{77}) - n_{57}^2$ . Thus the HOMO band is denoted by  $E_N(\alpha, B)$  while  $E_{N+1}(\alpha, B)$  corresponds to the LUMO band. The circles, lines and arrows in Fig.4 and Fig.5 have same meanings with those in Fig.3. Firstly we consider the magnetic moment under only AB flux  $M_{AB}$ . It is analogous to eq.(8) as

$$M_{AB} = -C_2 \sum_{l,j=occ} (dE_l(\alpha, 0)/d\alpha)|_{\alpha=\alpha_j} \quad (9)$$

with  $C_2$  defined in eq.(2). The HOMO and LUMO bands of type 2 is similar to those of metallic CNTs, but the band crossing point is slightly shifted from  $\alpha = \pm 2\pi/3$  owing to the phase shift at the disclinations. [14] Therefore the HOL is fully occupied and the GOP does not occur. Under finite  $B$ , however,  $\alpha_2 = 2\pi/3 + C_2B$  comes at the cross point so that  $M_{AB}$  shows a discrete change from negative to positive as shown by Fig.6. Contrary to it, HOL can be partially occupied in the CNT torus of type 3 and 4-1, on the condition that the corresponding periodic CNT junction is semi-metallic. Figure 5 is an example of it where  $E_N$  at  $\alpha = 0$  is vacant and  $E_{N+1}$  at  $\alpha = \pm\pi/3$  are partially occupied instead. The AB flux lifts the degeneracy of Hogs and only the lowered level at  $\alpha = \pi/3$  is occupied causing the GOP. Then does the direct flux reduce the GOP? Surprisingly, it *enhances* the GOP. The dashed lines in Fig.5 represent the dispersion relation  $E_l(\alpha, B)$  under the finite magnetic field  $B = 0.01\phi_0/a^2$ . In contrast to Fig.3, the dispersion lines is shifted along the  $\alpha$  axis rather than along the  $E$  axis. By this horizontal shift, the effect of the AB shift is not canceled but enhanced.

Here we should notice the competition between the GOP and spin paramagnetism. When the Zeeman split  $g\mu_B B$  ( $\mu_B =$  Bohr magneton,  $g \simeq 2$ ) is larger than the GOP split  $|MB| = |BdE/dB|$ , both the HOLs with positive  $dE/dk$  and negative  $dE/dk$  become occupied by the same spin so that spin magnetic moment, that is  $2g\mu_B$  per torus, appears instead of the GOP. Since  $\mu_B \simeq ta^2/\phi_0$  ( $t \simeq 3$  eV,  $a \simeq 0.25$  nm), the GOP is relevant when  $M$  is

larger than  $4t/(\phi_0/a^2)$ . To search the polygonal CNT torus showing the relevant GOP, the magnetic moment  $M(1.5\Delta B) = -(U(2\Delta B) - U(\Delta B))/\Delta B$  with  $\Delta B = 0.5 \times 10^{-5} \phi_0/a^2$ , i.e.,  $B = 1.5\Delta B \simeq 0.24$  Tesla, is calculated for two hundred seven kinds of the tori in the range of the parameters  $3 \leq n_S \leq 12$ ,  $1 \leq n_{75} \leq 6$ ,  $3 \leq n_L \leq 12$  and  $1 \leq n_{77} = (n_L - n_{75})/2 \leq 6$ . Among the two hundred seven tori, the number of the tori with  $M$  larger than  $4ta^2/\phi_0$  is twenty one. All of them belong to type 3 or type 4-1 and show the GOP. Especially three CNT tori show  $M$  larger than  $20ta^2/\phi_0$ . In contrast to it,  $M$  is much less than  $4ta^2/\phi_0$  for the tori without the GOP. Since  $MB$  is approximately the split between the degenerate HOL induced by  $B$ , temperature has to be lower than  $MB$ . When  $M = 20t/(\phi_0/a^2)$  and  $B = 1.5\Delta B$ ,  $MB \sim 6$  K, which is achievable in the experiment.

To show the distribution of  $M$  and the enhancement of  $M$  by the direct flux,  $M_{AB}/M$  is shown in Fig.7 as a function of  $M$  for the tori showing the relevant GOP. For all the tori,  $M_{AB} < M$ , i.e., the direct flux enhances the GOP. Figure 7 also shows that  $(|\vec{S}|^2/|\vec{S}_2|^2)M_{AB}/M$  becomes closer to unity than  $M_{AB}/M$  where the factor  $|\vec{S}|^2/|\vec{S}_2|^2$  represents the ratio of the AB flux to the full flux. This suggests that the effect of the direct flux can be almost included by the AB effect for which the cross section is not  $3\sqrt{3}|\vec{S}_2|^2/2$  but  $3\sqrt{3}|\vec{S}|^2/2$ . It is equivalent to replacing  $C_1$  and  $C_2$  in eq.(2) with  $C_1 = 0$  and  $C_2 = \sqrt{3}\pi|\vec{S}|^2/(2\phi_0)$ . In other word, the HOMO and LUMO dispersion curve can be approximated by

$$E_l(\alpha, B) \simeq E_l(\alpha + (\pi/3)(BS_D/\phi_0), 0) \quad (10)$$

with the cross section of the graphite plane  $S_D = 3\sqrt{3}(|\vec{S}|^2 - |\vec{S}_2|^2)/2$ . In fact, the shift of  $\alpha$  in eq.(10) can be seen in Fig.4 and Fig.5 where the dashed lines represent the dispersion relation  $E_l(\alpha, B = 0.01\phi_0/a^2)$ . It is also the effect of eq.(10) that the magnetic moment  $M$  shows discrete change at lower  $B$  than  $M_{AB}$  in Fig.6.

#### IV. SUMMARY AND DISCUSSION

In some of the polygonal CNT tori, the persistent current leads to large positive magnetic susceptibility inversely proportional to the temperature, which we call the giant orbital paramagnetism (GOP). The magnetic moment per torus can be larger than Bohr magneton in the achievable condition,  $B \sim 0.24$  Tesla and  $T < 6$  K. The necessary condition for the GOP is that the corresponding periodic CNT junction is semi-metallic, i.e., type 3 or type 4-1. The magnetic flux is divided into two parts which are the AB flux in the inner hole and the direct flux intersecting the graphite plane. In spite of the diamagnetism of the graphite, the direct flux enhances the GOP and its effect can be effectively included in the AB effect, where the cross section of the AB flux is not the inner hole area, but the area surrounded by the outer fringe, as shown in eq. (10) and Fig.7.

The GOP of the circular CNT torus is caused by the metallic band structure of the straight CNT, whereas that of the polygonal CNT torus originates from the semi-metallic band structures of the periodic CNT junction. This difference comes from change of the bond network, i.e., removing the shaded areas and sticking their edges in the projection map illustrated by Fig.2. Compared to it, the elastic deformation does not affect whether  $n$  and  $m$  are bonded or not, so it is irrelevant to the GOP of the polygonal CNT torus. Owing to this new kind of the GOP, the polygonal CNT torus is a promising nano-structure to realize the large persistent current.

#### V. ACKNOWLEDGMENT

This work was supported in part by a Grant-in-Aid for Creative Scientific Research on "Devices on molecular and DNA levels" (No. 13GS0017) from the Japan Society for the Promotion of Science.

FIGURES

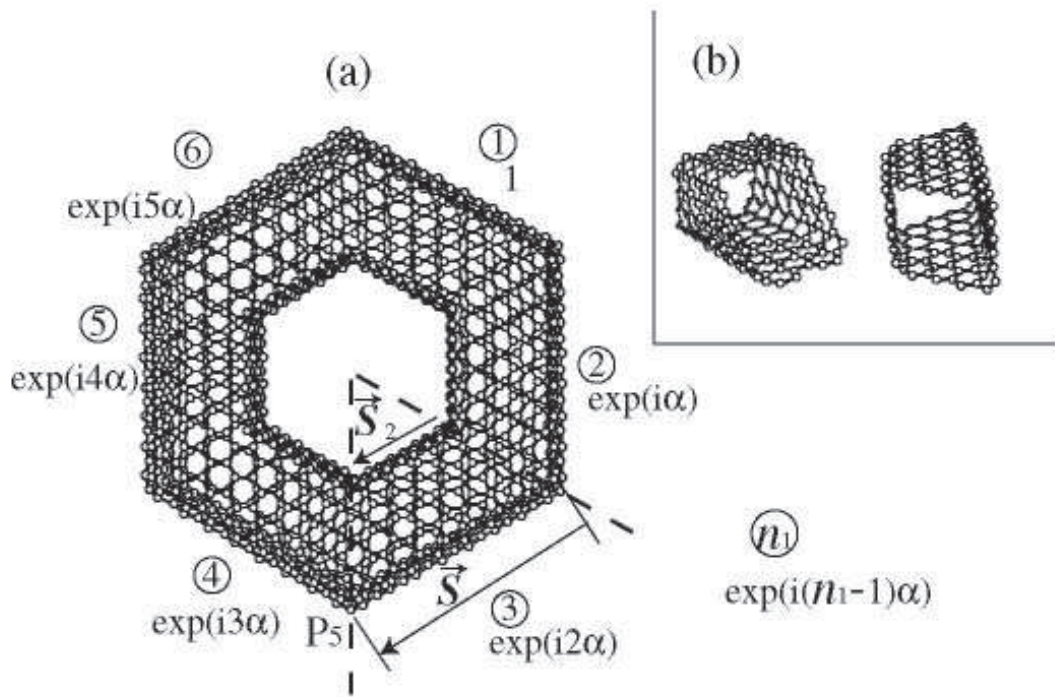


FIG. 1. (a) Three dimensional shape of the polygonal nanotube torus. The applied uniform magnetic field is perpendicular to this page. Labels of unit cells  $n_1$  are shown. (b) The unit cell of the CNT torus. The torus is composed of the six unit cells.

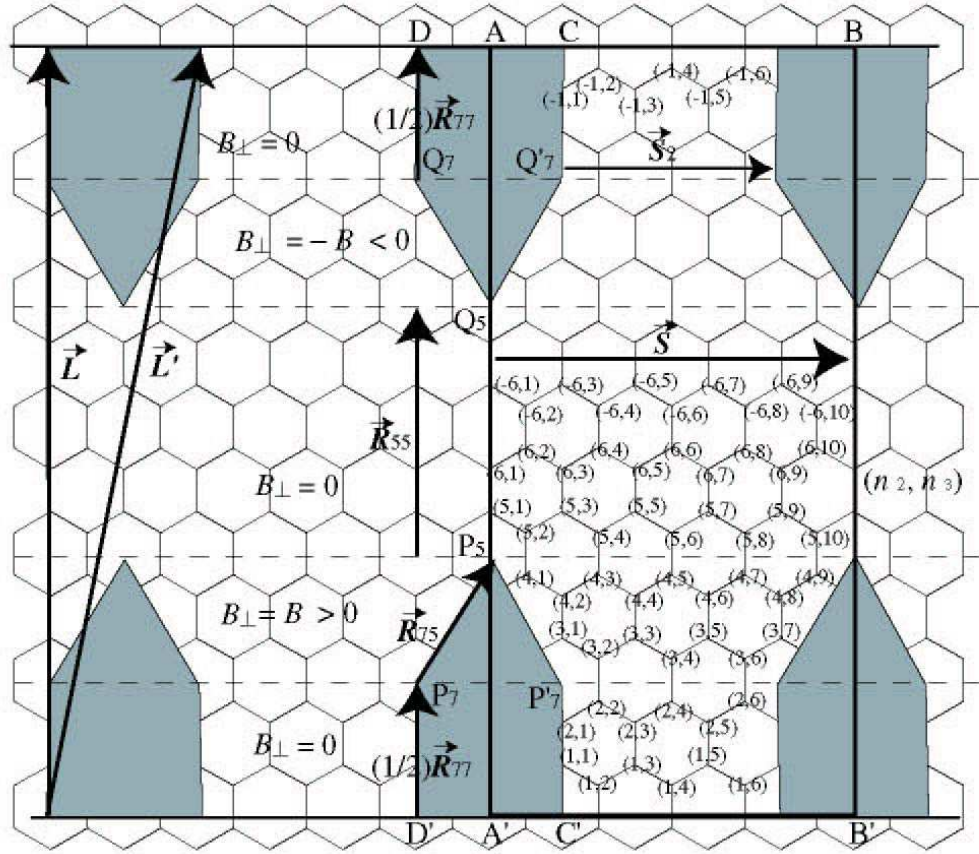


FIG. 2. Projection map of the CNT torus. The right rectangle is the unit cell. Magnetic field perpendicular to this page is denoted by  $B_{\perp}$ . Labels of atoms  $(n_2, n_3)$  in the unit cell are shown.

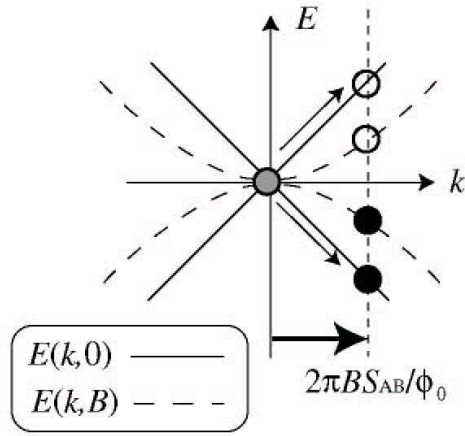


FIG. 3. The solid lines and dashed curves represent the dispersion relation without and with the direct flux, respectively. When the magnetic field  $B$  equals zero, the highest occupied level (HOL) of the torus is at the crossing of the solid lines as indicated by the gray circle. It is degenerate and partially occupied. Under finite  $B$ , the degeneracy is lifted and only the lower level (closed circle) is occupied while the higher level becomes vacant (open circle). The arrow indicates the change of the levels induced by the AB effect.



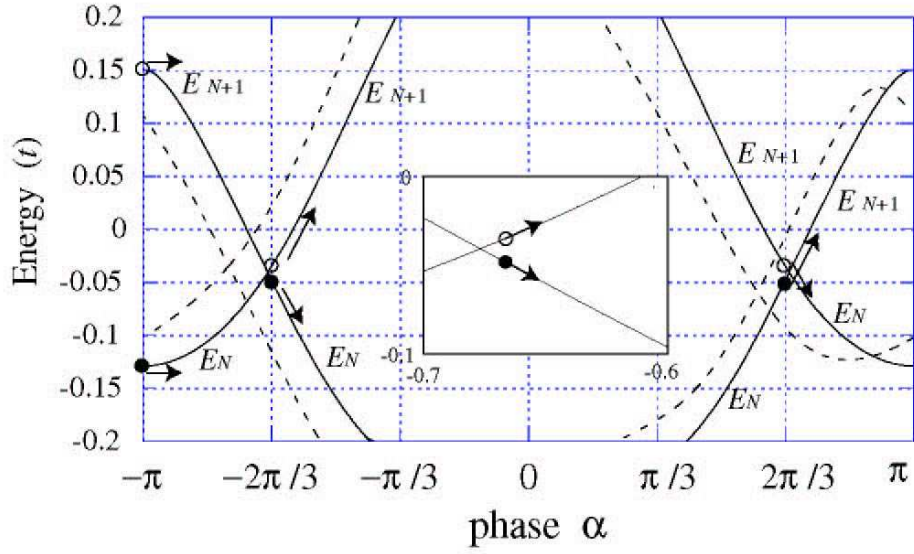


FIG. 4. The band structure of the periodic CNT junction of type 2 with the parameters  $(n_S, n_L, n_{75}, n_{55}) = (5, 7, 3, 2)$ . The circles, lines and arrows have the same meanings with Fig.3. For the dashed lines,  $B = 0.01\phi_0/a^2$ . Inset is the magnified band structure near the highest occupied level (HOL),  $E_N(-2\pi/3, 0)$ .

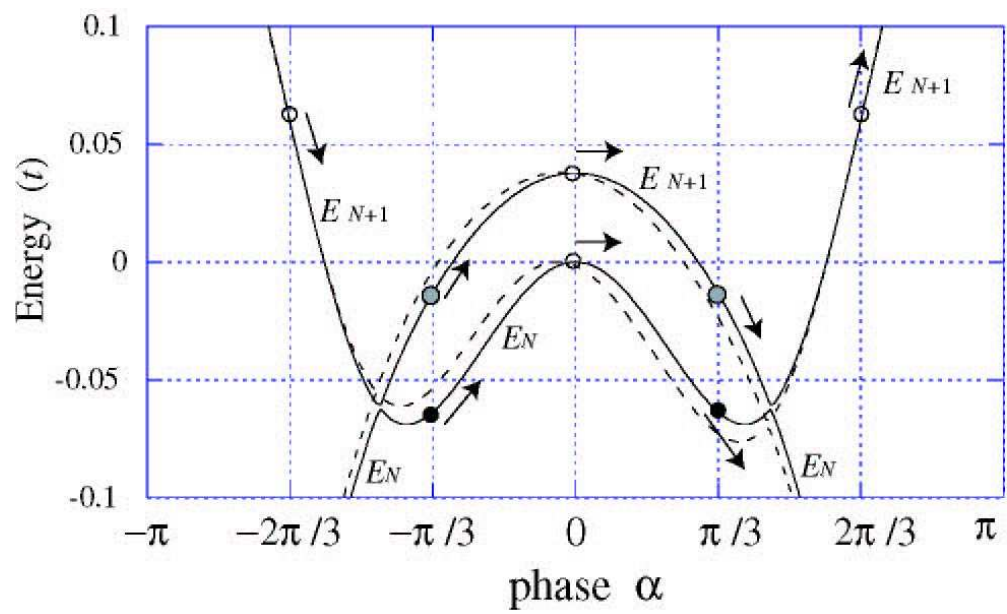


FIG. 5. The band structure of the periodic CNT junction of type 3 with the parameters  $(n_S, n_L, n_{75}, n_{55}) = (3, 7, 1, 3)$ . The circles, lines and arrows have the same meanings with Fig.3. For the dashed lines,  $B = 0.01\phi_0/a^2$ .

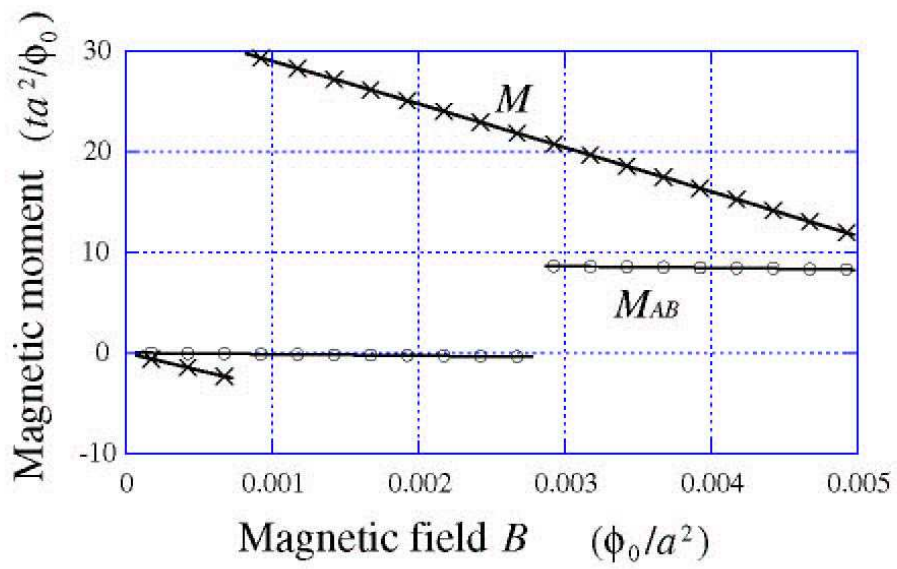


FIG. 6. The magnetic moments of the same periodic CNT junction as that in Fig.4, i.e.,  $(n_S, n_L, n_{75}, n_{55}) = (5, 7, 3, 2)$ , as a function of the magnetic field  $B$ . Here  $M$  and  $M_{AB}$  denote the magnetic moment induced by full flux and that induced by only AB flux, respectively. The former is calculated by the total energy  $U(B)$  as  $M((j - 0.5)\Delta B) = -(U(j\Delta B) - U((j - 1)\Delta B))/\Delta B$  with  $\Delta B = 0.5 \times 10^{-5}(\phi_0/a^2)$  and  $j = 1, 2, \dots, 100$ . For  $M_{AB}$ , the total energy is calculated by the Hamiltonian where  $\gamma^D$  in eq.(2) is replaced by zero.

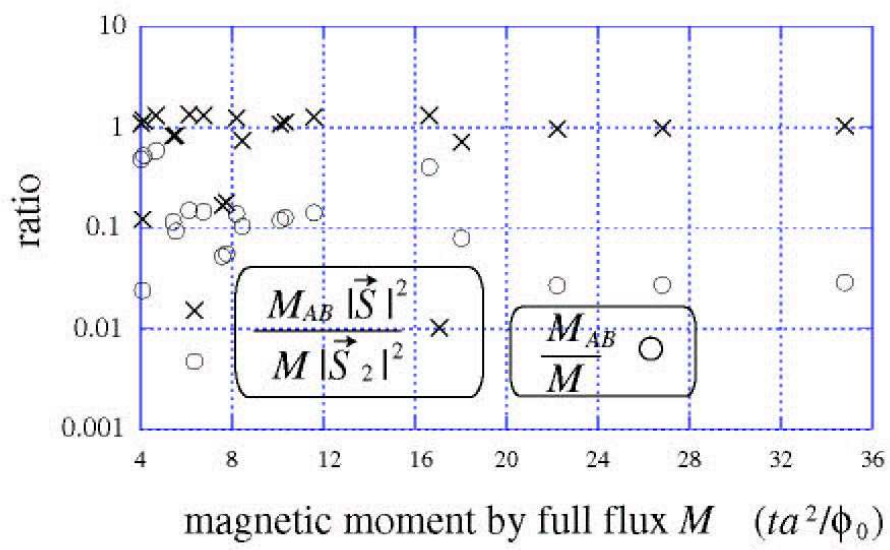


FIG. 7. The ratio  $M_{AB}/M$  and  $(|\vec{S}|^2/|\vec{S}_2|^2)M_{AB}/M$  as a function of  $M$  for the twenty one CNT tori with  $M$  larger than  $4ta^2/\phi_0$ . Here  $M$  and  $M_{AB}$  denote the magnetic moment induced by full flux and that induced by only AB flux, respectively. The applied magnetic field  $B$  equals  $0.75 \times 10^{-5} \phi_0/a^2$ . The factor  $|\vec{S}|^2/|\vec{S}_2|^2$  means the ratio of the full flux to the AB flux.

## REFERENCES

- [1] N. Hamada, S. I. Sawada, and A. Oshiyama, Phys. Rev. Lett. **68**, 1579 (1992); J. W. Mintmire, B. I. Dunlap, and C. T. White, *ibid* **68**, 631 (1992); R. Saito, M. Fujita, G. Dresselhaus, and M. S. Dresselhaus, Phys. Rev. B **46**, 1804 (1992).
- [2] D. Loss and P. Goldbart, Phys. Rev. B **43** 13762 (1991).
- [3] H. F. Cheung, Y. Gefen, and E. K. Riedel and W. H. Shih, Phys. Rev. B **37**, 6050 (1988)
- [4] M. F. Lin and D. S. Chuu, Phys. Rev. B **57**, 6731 (1998).
- [5] S. J. Tans and C. Dekker, Nature **385**, 780 (1997); R. Martel, H. R. Shea, and P. Avouris, *ibid* **398**, 780 (1997); H. R. Shea, R. Martel, and P. Avouris, Phys. Rev. Lett. **84**, 4441 (2000).
- [6] H. Ajiki and T. Ando, J. Phys. Soc. Jpn. **62** 2470 (1993); *ibid* **63** 4267 (1994).
- [7] L. P. Levy, G. Dolan, J. Dunsmuir and H. Bouchiat, Phys. Rev. Lett. **64**, 2074 (1990); V. Chandrasekhar, R. A. Webb, M. J. Brady, M. B. Ketchen, W. J. Gallagher and A. Kleinsasser, *ibid* **67**, 3578 (1991); D. Mailly, C. Chapelier and A. Benoit, *ibid* **70**, 2020 (1993);
- [8] S. Latil, S. Roche and A. Rubio, Phys. Rev. B **67**, 165420 (2003)
- [9] A. Latgé, C. G. Rocha, L.A.L. Wanderley, M. Pacheco, P. Orellana and Z. Barticevic. Phys. Rev. B **67** 155413 (2003).
- [10] V. Meunier, P. Lambin and A. A. Lucas, Phys. Rev. B **57** 14886 (1998).
- [11] R. Tamura, Phys. Rev. B. **67**, 121408 (2003); *ibid.* **64**, 201404 (2001); R. Tamura and M. Tsukada, *ibid.* **61**, 8548 (2000); H. Matsumura and T. Ando, J. Phys. Soc. Jpn. **67**, 3542 (1998); L. Chico, Vincent H. Crespi, Lorin X. Benedict, Steven G. Louie, and Marvin L. Cohen, Phys. Rev. Lett. **76**, 971 (1996).



- [12] R. Tamura and M. Tsukada, Phys. Rev. B **52**, 6015 (1995); Y. Kasahara, R. Tamura and M. Tsukada, Phys. Rev. B. **67**, 115419 (2003); T. Yaguchi and T. Ando, J. Phys. Soc. Jpn, **70** 1327 (2001).
- [13] K. Akagi, R. Tamura, M. Tsukada, S. Itoh, and S. Ihara, Phys. Rev. B **53**, 2114 (1996).
- [14] R. Tamura and M. Tsukada, J. Phys. Soc. Jpn. **68**, 910 (1999). Phys er, Rabani d, E.
- [15] S. Itoh and S. Ihara, Phys. Rev. B **48**, 8323 (1993);B. I. Dunlap, *ibid* **46**, 1933 (1992); D. H. Oh, J. M. Park and K. S. Kim, *ibid* **62**, 1600 (2000).
- [16] R. C. Haddon, Nature **388**, 31 (1997).
- [17] O. Hod, E. Rabani and R. Rev. B **67**, 195408 (2003)
- [18] H. Ajiki and T. Ando, J. Phys. Soc. Jpn. **65** 505 (1995).
- [19] Though we reported that the periodic CNT junctions of type 3 and type4-1 are semi-metallic in Ref. [13], we found later that they can be also semi-conducting and metallic.